Protein Science (2000), *9*:2161–2169. Cambridge University Press. Printed in the USA.

Solution structure of DinI provides insight into its mode of RecA inactivation

BENJAMIN E. RAMIREZ,[1] OLEG N. VOLOSHIN,[2] R. DANIEL CAMERINI-OTERO,[2] AND AD BAX[1,3]

[1]Laboratory of Chemical Physics, National Institutes of Diabetes and Digestive and Kidney Diseases, National Institutes of Health, Bethesda, Maryland 20892-0520
[2]Genetics and Biochemistry Branch, National Institutes of Diabetes and Digestive and Kidney Diseases, National Institutes of Health, Bethesda, Maryland 20892-0520

(RECEIVED May 30, 2000; FINAL REVISION August 15, 2000; ACCEPTED August 24, 2000)

Abstract

The *Escherichia coli* RecA protein triggers both DNA repair and mutagenesis in a process known as the SOS response. The 81-residue *E. coli* protein DinI inhibits activity of RecA in vivo. The solution structure of DinI has been determined by multidimensional triple resonance NMR spectroscopy, using restraints derived from two sets of residual dipolar couplings, obtained in bicelle and phage media, supplemented with J couplings and a moderate number of NOE restraints. DinI has an α/β fold comprised of a three-stranded β-sheet and two α-helices. The β-sheet topology is unusual: the central strand is flanked by a parallel and an antiparallel strand and the sheet is remarkably flat. The structure of DinI shows that six negatively charged Glu and Asp residues on DinI's kinked C-terminal α-helix form an extended, negatively charged ridge. We propose that this ridge mimics the electrostatic character of the DNA phosphodiester backbone, thereby enabling DinI to compete with single-stranded DNA for RecA binding. Biochemical data confirm that DinI is able to displace ssDNA from RecA.

Keywords: bicelle; DinI; dipolar coupling; liquid crystal; NMR; Pf1; RecA

Maintaining a stable genome is essential for the survival of an organism. For this reason, it is critical that an organism possesses some mechanism that repairs DNA damage. DNA damage prevents replication by DNA polymerases, resulting in the formation of single-stranded DNA (ssDNA). In *Escherichia coli*, binding of the RecA protein to ssDNA induces a DNA repair process known as the SOS response (Friedberg et al., 1995). Once RecA binds to ssDNA, the ssDNA-RecA cofilament acts as a coprotease, promoting the autocleavage of the LexA repressor. This cleavage event inactivates LexA, resulting in the expression of the 30 or so proteins that are the constituents of the SOS response. Faithful repair, that is, repair without introducing mutations, is a result of recombinational repair mediated by RecA and other proteins in the SOS response (Cox, 2000). If these error free processes fail to repair the damage, additional SOS proteins activate so-called translesion DNA synthesis, which enables DNA replication to proceed even at damaged sites (Walker, 1998). This error-prone process is referred to as SOS mutagenesis, because mutations arise by the incorporation of random bases. SOS mutagenesis is also induced by the coprotease activity of the ssDNA-RecA cofilament, because one of the proteins involved in this process, UmuD, is active only after RecA-mediated autocleavage (Shinagawa et al., 1988). Clearly, the coprotease activity of ssDNA–RecA cofilament plays a pivotal role in inducing DNA repair and mutagenesis.

One of the SOS proteins synthesized upon inactivation of LexA is a small 81-residue protein known as DinI, which inhibits the coprotease activity of RecA (Yasuda et al., 1998). When DinI is overexpressed, stimulation of the SOS response by mitomycin C and autocleavage of LexA and UmuD are blunted in vivo (Yasuda et al., 1998). The mechanism of how DinI down regulates the SOS response was not determined. However, recent biochemical data indicate that DinI can prevent ssDNA binding to RecA and can even displace ssDNA from ssDNA–RecA cofilaments (O.N. Voloshin, B.E. Ramirez, A. Bax, & R.D. Camerini-Otero, in prep.).

We have determined the solution structure of DinI in an effort to understand the mechanism through which it inhibits RecA coprotease activity. Although conventional multidimensional NMR is adequate to define the structure of a small protein such as DinI at an adequate level of resolution, the present structure determination relied primarily on structural restraints derived from residual dipolar couplings, measured in two liquid crystalline media. Dipolar couplings have been shown to significantly improve the accuracy of structures determined by NMR, as exemplified by an increase of the number of residues that lie in the most-favored regions of the Ramachandran plot (Tjandra et al., 1997), improved agreement with structure-predicted chemical shift changes (Ottiger et al., 1997),

Reprint requests to: Ad Bax, NIH, Building 5, Rm. 126, Bethesda, Maryland 20892; e-mail: bax@nih.gov.

and closer agreement with crystal structures in cases where these are available (Clore et al., 1999). Residual dipolar couplings result from the weak alignment with the magnetic field of a protein dissolved in an aqueous, dilute liquid crystalline (LC) medium. Such LC media consist of large, magnetically oriented particles (Tjandra & Bax, 1997a). Dipolar couplings are a function of the orientation of the internuclear vector relative to the molecular alignment tensor, and hence, provide structural information that is distinctly different from other NMR data such as nuclear Overhauser effects (NOEs), coupling constants, or chemical shifts.

A single alignment tensor restricts the internuclear vector orientation to one of two cones that are related by inversion symmetry. This degeneracy can be greatly reduced by measuring dipolar couplings for a second alignment tensor orientation (Ramirez & Bax, 1998). With two independent alignment tensors, the number of possible internuclear orientations are limited to the points where the corresponding cones intersect. The most commonly used LC media in biomolecular NMR are either planar phospholipid micelle disks, commonly known as bicelles (Sanders & Schwonek, 1992; Tjandra & Bax, 1997a; Vold et al., 1997), and filamentous phage (Clore et al., 1998b; Hansen et al., 1998). In the medium containing nearly neutral bicelles, protein alignment is dominated by steric interactions. Instead, in the strongly negatively charged filamentous phage medium electrostatic interactions frequently dominate (Zweckstetter & Bax, 2000). Consequently, proteins will align differently in bicelle and phage LC media, yielding independent alignment tensors (Clore et al., 1998b). The DinI structure was calculated from these combined sets of dipolar couplings, measured in bicelle and phage media, supplemented by a moderate number of NOE and J-coupling derived torsion angle restraints.

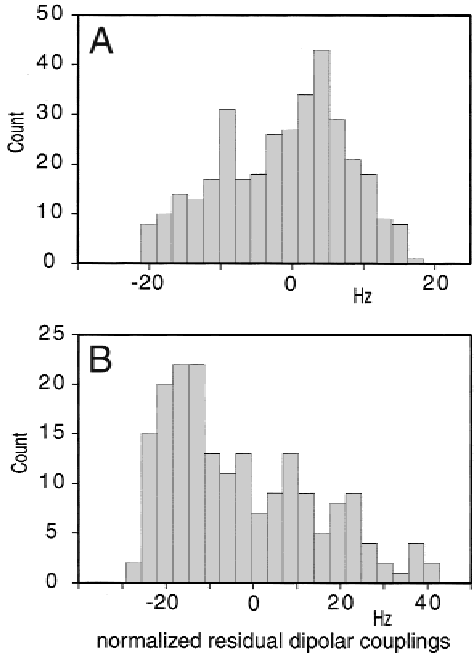

Fig. 1. Histogram of $^1D_{NH}$, $^1D_{C\alpha H\alpha}$, $^2D_{C'HN}$, $^1D_{C'N}$, and $^1D_{C\alpha C'}$ residual dipolar couplings. The $^1D_{C\alpha H\alpha}$, $^2D_{C'HN}$, $^1D_{C'N}$, and $^1D_{C\alpha C'}$ couplings were normalized to match those of the $^1D_{NH}$ couplings, using scaling factors of 0.50, 3.2, 8.2, and 5.0, respectively (Ottiger & Bax, 1998b). **A:** Residual dipolar couplings obtained in a LC solution consisting of 5% bicelle LC (30:10:1 DTPC:DHPC:CTAB) and 100 mM NaCl. **B:** Residual dipolar couplings obtained in a LC solution consisting of ~8 mg/mL Pf1 phage and 150 mM NaCl. For the Pf1 sample, only the $^1D_{NH}$, $^1D_{C\alpha H\alpha}$, and $^1D_{C\alpha C'}$ couplings were measured for reasons discussed in the text.

Results and discussion

The structure of DinI was determined from heteronuclear multidimensional NMR data acquired from uniformly labeled ^{15}N and $^{13}C/^{15}N$ samples. At 1 mM, the average backbone amide ^{15}N transverse relaxation time T_2 equals ~85 ms, considerably shorter than the ~150 ms expected for a monomeric 9 kD globular protein. Adding salt markedly decreases τ_C, which is further reduced by decreasing the protein concentration. As a compromise, all experiments were performed at 0.6 mM DinI and 100 mM NaCl (T_2 = ~130 ms), unless specified otherwise. A sample at pH 6.6 and a temperature of 25 °C yielded the best dispersion and most uniform peak intensity in the ^{15}N-^1H heteronuclear single quantum coherence (HSQC) spectrum. At 35 °C, a number of resonances in the ^{15}N-HSQC spectrum broadened significantly.

$^1D_{NH}$, $^1D_{NC'}$, $^2D_{C'HN}$, $^1D_{C\alpha H\alpha}$, and $^1D_{C\alpha C'}$ residual dipolar couplings were measured for DinI dissolved in bicelle LC media. Approximate values for the axial (D_a) and rhombic (D_r) components of DinI's alignment tensor in the bicelle medium were determined from the normalized distribution of all the observed residual dipolar couplings (Fig. 1A) (Clore et al., 1998a). Initial values were $D_a = -10.5$ Hz (normalized for $^1D_{NH}$) and $R = 0.38$ ($R = D_r/D_a$). D_a and R were subsequently refined by conducting a grid search to find values that yield the lowest energy structures. Final values were $D_a = -10.0$ Hz and $R = 0.28$.

A second set of $^1D_{NH}$, $^1D_{C\alpha H\alpha}$, and $^1D_{C\alpha C'}$ residual dipolar couplings was recorded for DinI dissolved in the Pf1 filamentous phage LC medium. $^{13}C^\alpha$-{$^1H^\alpha$} doublets obtained from the three-dimensional (3D) constant time (HA)CA(CO)NH triple resonance experiment for a helical segment of DinI in the isotropic, bicelle LC, and phage LC media are compared in Figure 2. Initial values for the D_a and R were again determined from the normalized distribution of these observed residual dipolar couplings (Fig. 1B), yielding $D_a = 21.0$ Hz and $R = 0.19$. Subsequent refinement of these values by conducting a grid search yielded $D_a = 22.0$ Hz and $R = 0.09$. The alignment tensors determined in the phage LC and bicelle LC are quite different, as judged by the lack of correlation between $^1D_{NH}$ residual dipolar couplings observed in these two media (Fig. 3).

A total of 1,786 experimental NMR restraints were used in a simulated annealing algorithm to determine the 3D structure of

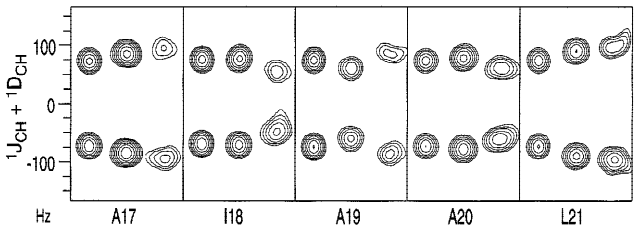

Fig. 2. Small sections taken from the 3D (HA)CA(CO)NH spectra for residues A17–L21, showing $^{13}C^\alpha$-{$^1H^\alpha$} doublets in the isotropic (left), bicelle-aligned (center) and phage-aligned (right) 3D constant-time (HA)CA(CO)NH spectra for residues A17–A22. These residues form the beginning of DinI's first α-helix, and the residual dipolar couplings exhibit the periodicity characteristic of a regular α-helix.

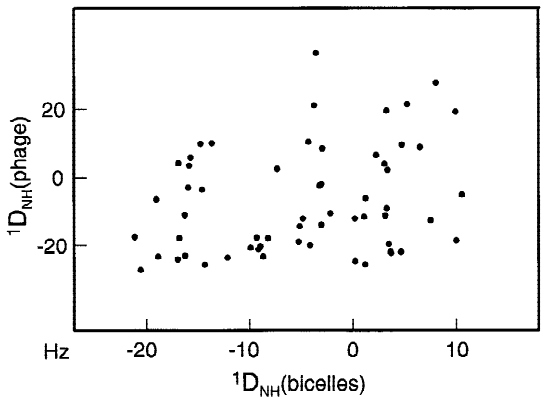

Fig. 3. Correlation between the $^1D_{NH}$ residual dipolar couplings recorded in bicelle and phage LC media. The lack of correlation illustrates the different orientations of the alignment tensor in the phage LC. In the bicelle alignment tensor frame, the phage alignment tensor is characterized by Euler angles $\alpha = 115°$; $\beta = 89°$; $\gamma = 20°$.

DinI. These restraints included 333 residual dipolar couplings ($^1D_{NH}$, $^1D_{NC'}$, $^2D_{C'HN}$, $^1D_{C\alpha H\alpha}$, and $^1D_{C\alpha C'}$) obtained from the bicelle LC sample and 192 residual dipolar couplings ($^1D_{NH}$, $^1D_{C\alpha H\alpha}$, and $^1D_{C\alpha C'}$) obtained from the phage LC sample. There are 1,114 NOE restraints, including 59 ambiguous NOEs, and only 140 of the unique restraints are long range. No extensive effort was made to collect long-range NOE restraints. Rather, we relied on the dipolar restraints to provide both accuracy and precision. Nevertheless, we also measured $^3J_{C'C\gamma}$ $^3J_{NC\gamma}$ for all the Ile, Thr, Val, and aromatic residues to ensure selection of the correct side-chain conformation. These experiments are relatively rapid and are also straightforward to interpret. Unique χ_1 angles were found for all residues, except T6, Y31, H39, and V79, which exhibit $^3J_{C'C\gamma}$ and $^3J_{NC\gamma}$ values indicative of χ_1 averaging. $^3J_{C'C\gamma}$ values for F33 could not be determined because it is followed by a Pro residue, but its very small $^3J_{NC\gamma}$ coupling rules out a $\chi_1 = 180°$ rotamer.

A superposition of the 15 final simulated annealing structures is shown in Figure 4. Although the precision of the backbone is very high (root-mean-square deviation (RMSD) = 0.17 Å), the RMSD is considerably higher when all non-H atoms are included (0.84 Å). It is well known that the precision at which an NMR structure is determined frequently is considerably higher than its accuracy. However, we believe the quality of the DinI structure to be quite good as it yields favorable scores when cross-validated using Q-factor analysis (see below). Moreover, when evaluated by the program PROCHECK (Laskowski et al., 1993), the overall quality indicators also score relatively high. For example, even if the potential for driving backbone torsion angles to the regions most populated in the Protein Data Bank (PDB) (Kuszewski et al., 1997) is turned off, about 90% of the residues have backbone torsion angles in the most favored region of the Ramachandran map, with no residues in the generously allowed or disallowed regions. Table 1 provides a summary of the structural statistics.

Description of the structure

DinI possesses an α-β fold (Fig. 5), where two α-helices (residues 17–32 and 57–78) pack against a three-stranded β-sheet (residues 1–8, 40–44, 48–53). The β-sheet is unusual in that the central,

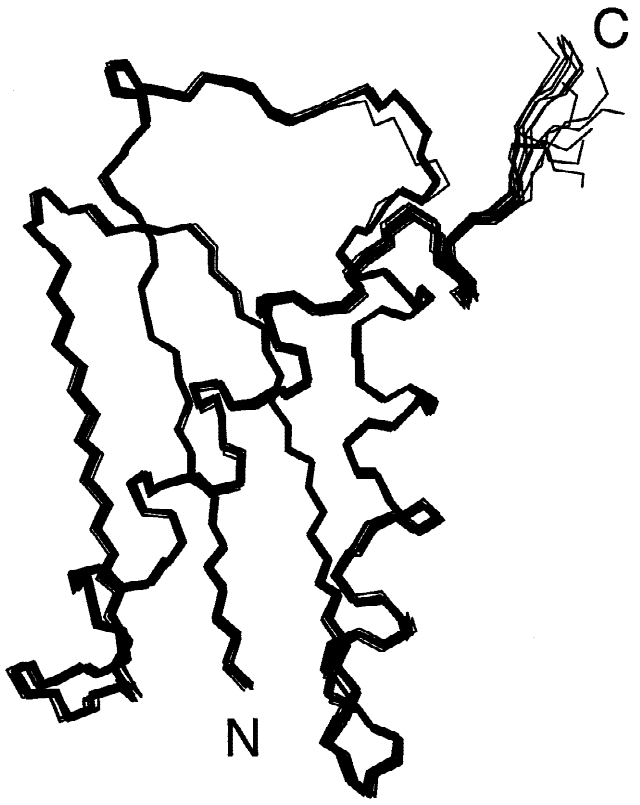

Fig. 4. Backbone superposition of the final 15 DinI structures calculated by simulated annealing.

N-terminal strand is flanked by both an antiparallel and a parallel strand, and is remarkably flat. The central, N-terminal strand is connected to the first α-helix via a segment that contains the sequence SPLP. The number of dipolar restraints per residue in this region is much smaller because most of the backbone dipolar coupling measurements rely on detection of the H^N signal, which is absent for Pro residues. Therefore, more careful analysis of NOEs in this region was essential for ensuring the correct local geometry in this region. Strong H^{α}_{i-1} − Pro$_i$-H^{δ} NOEs for all three prolyl residues in DinI indicated *trans* peptide bonds. This information can be difficult to extract unambiguously from dipolar restraints, particularly in view of the fact that the number of measurable backbone dipolar couplings for Pro residues is much reduced.

Strand β1 is followed by a long α-helix (A17–A32) that is capped by F33. Most of the F33 phenyl ring is exposed to solvent, although it also shows some long-range NOEs to residues such as M1 and I63. The connection between this α-helix and strand β2 (V40–Y44) is well defined, with no evidence of conformational exchange contributions. The outside strands of the three-stranded β-sheet are connected by a three-alanine linker, A45–A46–A47. The amide of A46 is not observable in the ^{15}N-^{1}H HSQC spectrum as a result of conformational exchange. The third β-strand (N48–I53) is well-defined and rigid, and is connected to the C-terminal helix (K57–F78) by a short three-residue sequence: G54–A55–T56. The amide of G54 is not observed in the ^{15}N-^{1}H HSQC spectrum, also as a result of conformational exchange.

The C-terminal α-helix displays a pronounced kink of ~70° at residues E72–S73–A74, which is the position where it crosses over

Table 1. *Structural statistics*[a]

RMSDs from experimental distance restraints (Å)[b]	
All (1114)	0.056 ± 0.001
Intraresidue (592)	0.063 ± 0.001
Interresidue sequential ($\|i-j\|=1$) (278)	0.038 ± 0.002
Interresidue short range ($1<\|i-j\|<5$) (104)	0.061 ± 0.002
Interresidue long range ($\|i-j\|>5$) (140)	0.051 ± 0.003
RMSDs from experimental dihedral restraints (deg) (148)[b]	0.65 ± 0.03
RMSDs from residual dipolar couplings (Hz)	
$^1D_{NH}$ (bicelle) (69)	1.14 ± 0.01
$^1D_{C\alpha H\alpha}$ (bicelle) (70)	1.99 ± 0.02
$^1D_{C\alpha C'}$ (bicelle) (69)	0.46 ± 0.01
$^1D_{NC'}$ (bicelle) (61)	0.32 ± 0.01
$^2D_{C'HN}$ (bicelle) (64)	0.89 ± 0.01
$^1D_{NH}$ (phage) (58)	1.28 ± 0.01
$^1D_{C\alpha H\alpha}$ (phage) (65)	2.55 ± 0.04
$^1D_{C\alpha C'}$ (phage) (69)	0.97 ± 0.01
Deviations from idealized covalent geometry	
Bonds (Å)	0.004 ± 0.0001
Angles (deg)	0.93 ± 0.01
Impropers (deg)	0.68 ± 0.01
E_{LJ} (kcal/mol)[c]	−355 ± 7.5
Coordinate precision (Å)[d]	
Backbone nonhydrogen atoms	0.17 ± 0.03
All nonhydrogen atoms	0.84 ± 0.06
PROCHECK quality indicators	
Residues in most-favored region of Ramachandran plot	97/89%[e]
No. of bad contacts	2/2

[a]Statistics are for the final 15 simulated annealing structures. The number of terms for the various restraints is given in parentheses. The final values for the force constants of the various terms in the simulated annealing target function are as follows: 1,000 kcal mol^{-1} Å^{-2} for bond lengths, 500 kcal mol^{-1} rad^{-2} for angles and improper torsions (which serve to maintain planarity and chirality), 4 kcal mol^{-1} Å^{-4} for the quartic Van der Waals repulsion term (with the van der Waals radii set to 0.8 times their value in CHARMM PARAM 19/20 parameters), 30 kcal mol^{-1} Å^{-2} for experimental distance restraints (interproton distances), 100 kcal mol^{-1} rad^{-2} for torsion angle restraints, 1.0 kcal mol^{-1} Hz^{-2} for the bicelle derived $^1D_{NH}$ dipolar coupling restraints, 0.25 kcal mol^{-1} Hz^{-2} for the $^1D_{C\alpha H\alpha}$ dipolar coupling restraints, 2.5 kcal mol^{-1} Hz^{-2} for the $^1D_{C\alpha C'}$ dipolar coupling restraints, 6.4 kcal mol^{-1} Hz^{-2} for the $^1D_{C'N}$ dipolar coupling restraints, 1.8 kcal mol^{-1} Hz^{-2} for the $^2D_{C'HN}$ dipolar coupling restraints. These force constants were divided by two for dipolar coupling restraints measured in phage, to account for the stronger alignment.

[b]None of the structures exhibited interproton distance violations greater than 0.5 Å or dihedral angle violations greater than 5°. Torsion angle restraints included 76 ϕ, 51 ψ, and 21 χ_1 angles.

[c]The Lennard–Jones van der Waals energy was calculated with the CHARMM PARAM 19/20 parameters and was not included in the simulated annealing target function.

[d]Defined as the average RMS difference (residues 2–78) between the final 15 simulated annealing structures and the mean coordinates.

[e]Eighty-nine percent for a separate series of calculations without inclusion of the Ramachandran term in the structure calculation. There were no ϕ/ψ angles in the generously allowed or disallowed region of the Ramachandran plot.

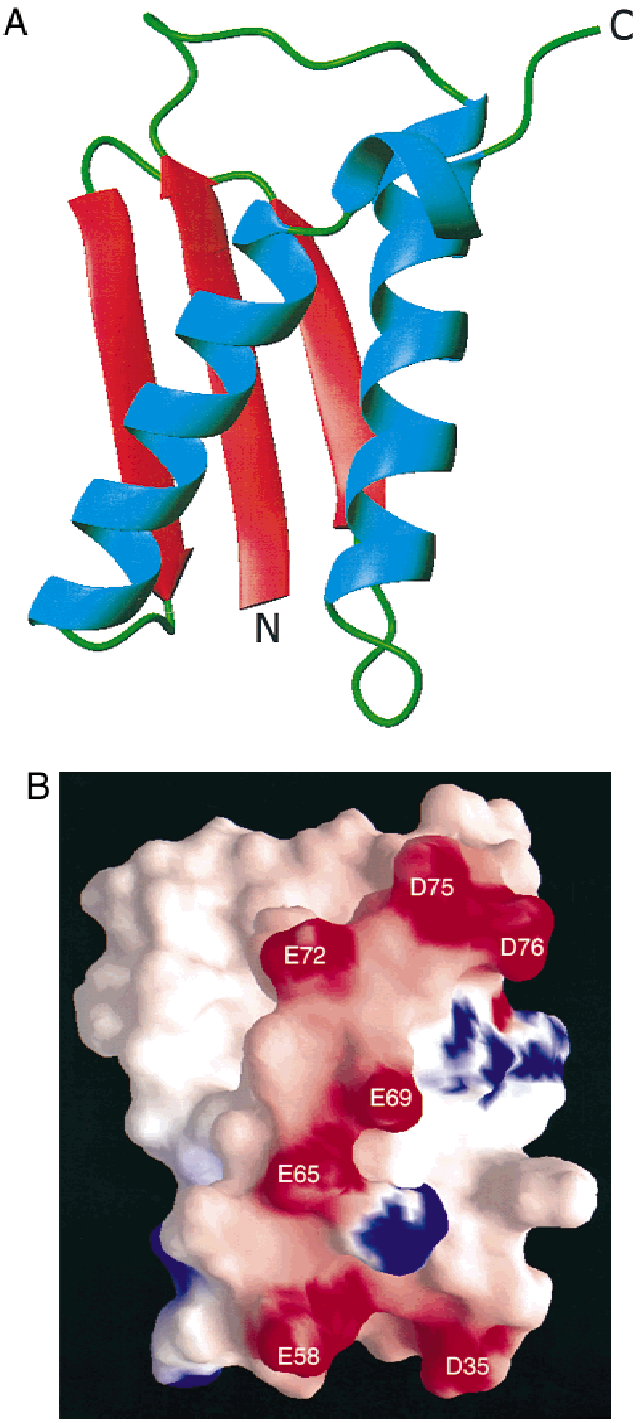

Fig. 5. A: Backbone ribbon diagram of DinI, with helices colored blue, β-strands red, and loops, turns and the flexible C-terminus in green. **B:** Map of the electrostatic surface potential. The electrostatic potential is colored from red (negative charge) to blue (positive charge). These figures were generated using the programs MOLMOL (Koradi et al., 1996) and GRASP (Nicholls et al., 1991).

the first α-helix. The presence of this kink is supported not only by secondary C$^\alpha$ shifts and $^3J_{HNH\alpha}$ couplings, but also by the $^1D_{NH}$ couplings: because all the N—H bonds in a helix point approximately in the same direction, $^1D_{NH}$ values for a straight helix tend to cluster in a narrow range. Residues 75–78 have a characteristic $^1D_{NH}$ coupling that differs significantly from the $^1D_{NH}$ values of residues 57–71. Short-range NOEs confirm the helical character for residues 75–78, and long-range NOEs between F77/W78 and

residues A17, A20, and L21 in the first α-helix confirm the orientation of this helical section. Backbone amides just prior to the kink region (T70–E72) are strongly attenuated by intermediate rate conformational exchange, and consequently, only exhibit very weak NOEs and decreased accuracy for the dipolar couplings, in particular for $^1D_{NC'}$, $^2D_{C'HN}$, and $^1D_{C\alpha C'}$. The dipolar couplings tightly define the orientation of the C-terminal helical segment (residues 74–78), however. No long-range NOEs are observed for the V79 methyl groups, in agreement with its χ_1 averaging noted above, and the backbone ^{15}N T_2 of the C-terminal residues S80 and E81 indicates extensive internal dynamics for these terminal two residues.

Similarity to other structures

Using the DALI program (Holm & Sander, 1993), we searched the PDB for proteins with folds similar to DinI. High similarity scores were found for segments of only two proteins: (1) residues P1-L102 of 5 carboxymethyl hydroxy muconate isomerase (1otg, Z = 5.3, RMSD = 2.6 Å, 6% identity) (Subramanya et al., 1996). However, compared to DinI, the order of the strand and helical segments is not identical. (2) The P2-S98 region of the cytokine d-dopachrome tautomerase (1dpt, Z = 5.0, RMSD = 2.8 Å, 17% identity) (Sugimoto et al., 1999). In contrast to DinI, neither protein is active in any processes involving DNA metabolism. Their remote structural similarity to DinI therefore is believed to be coincidental.

Interaction between DinI and the liquid crystal

Significant changes in the ^1H-^{15}N HSQC spectrum were observed between samples without and with bicelles. In fact, several resonances sharpened in the presence of bicelles (e.g., A15, L67, T70, and E72) but there was no evidence of a second set of resonances nor that the protein had denatured. To the contrary, the secondary C^α shifts of the protein in the bicelle medium indicated that the protein is slightly more structured, i.e., $^{13}C^\alpha$ chemical shifts for several α-helical residues (A17, A20, Q68, and A74) shifted further downfield, and small upfield shifts were observed for several β-sheet $^{13}C^\alpha$ resonances (T6, R43, and N48). The largest chemical shift changes occur for residues L67–D75 that include the kink in the C-terminal α-helix. This suggests that these chemical shift changes are caused by DHPC binding to DinI. This was confirmed by titrating a DinI sample with DHPC. At a DHPC concentration of 4 mM, the ^{15}N-HSQC spectrum was superimposable with the ^{15}N-HSQC spectrum recorded in the aligned bicelle medium. Interestingly, this concentration provides yet another, independent measure for the concentration of free DHPC in a bicelle LC solution, previously inferred from very different types of data (Ottiger & Bax, 1998a; Struppe & Vold, 1998). The DHPC titration experiments indicated a very weak K_d of ~2 mM. Titration of CT ^{13}C-HSQC spectra with DHPC allowed mapping of the resonances previously assigned in the bicelle-free medium. The assignment of the N and H^N resonances in the aligned state was also confirmed by the C^α and C' chemical shifts, measured in the 3D ^1H-coupled(F1) (H)CA(CO)NH and 3D $^{13}C^\alpha$-coupled (F1) HNCO experiments, respectively, which were needed for deriving the $D_{C\alpha H\alpha}$ and $D_{C'C\alpha}$ couplings. Although small changes in chemical shifts were evident for a number of these resonances, C^α and C' resonances generally were much less affected than amide resonances.

The residues of DinI most affected by the presence of DHPC were delineated by calculating the average chemical shift change that occurred in the presence of 10 mM DHPC (Fig. 6). The structure of DinI indicates the presence of two primarily hydrophobic pockets where DHPC may bind. The indole ring of W71 acts a barrier, separating the two pockets; L13, L21, W77, and F78 line the inside of one of the pockets, while V5, I7, L50, and L67 line the other one. Weak NOEs between DHPC and side chains of L13, I18, L21, W71, and W77 of DinI are present in NOE spectroscopy (NOESY) spectra, recorded in the presence of 10 mM DHPC. The low intensity of the intermolecular NOEs and the weak binding constant suggest that binding of DHPC to DinI is

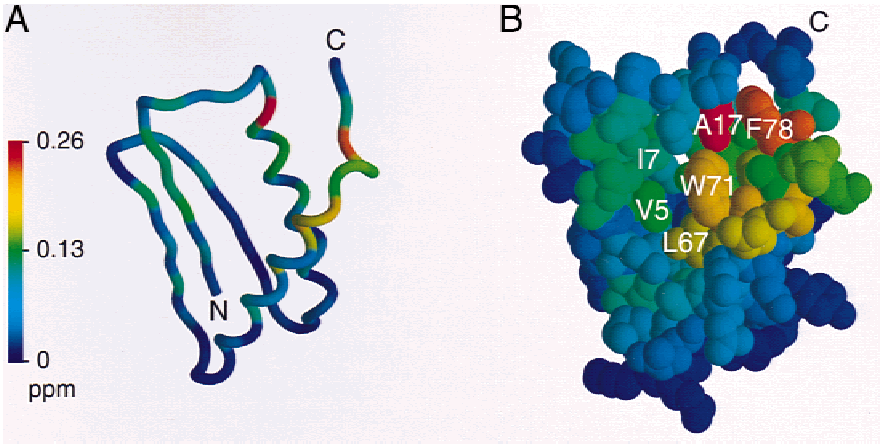

Fig. 6. (**A**) Worm and (**B**) space-filling models of DinI, color-coded to indicate chemical shift differences for each residue upon addition of 10 mM DHPC. Blue indicates residues with little to no change in chemical shifts while red denotes residues with the largest changes in chemical shifts. All assigned chemical shifts were used to calculate the chemical shift difference. The chemical shift changes $\Delta\delta$ of different nuclei were normalized and averaged on a per-residue basis (Grzesiek et al., 1997). Specifically, the average chemical shift difference for a given residue is calculated as $[\sum_i(\Delta\delta_i)^2/N]^{1/2}$, where the summation extends over all N nuclei i for which shifts were measured in a given residue, and ^{15}N and ^{13}C $\Delta\delta_i$ were scaled down by factors of 5 and 2, respectively, prior to calculating $[\sum_i(\Delta\delta_i)^2/N]^{1/2}$.

nonspecific, and therefore, no further effort was made to characterize the DinI–DHPC complex in more detail. Nevertheless, it is conceivable that the pockets where DHPC binds are important for other, yet unknown intermolecular interactions with other proteins or small molecules, which may modulate DinI–RecA affinity.

The relatively small magnitude of the chemical shift changes suggests that the DinI structure remains largely unchanged in the presence of DHPC. This is confirmed by residual dipolar couplings measured in the phage LC medium. No significant chemical shift changes relative to the isotropic sample are observed for DinI in the presence of Pf1. Alignment of DinI in the phage medium is dominated by electrostatic interactions, but no significant binding of DinI to the phage appears to take place. If such binding were to occur, the protein ^{15}N T_2 in the bound state would be extremely short, and exchange with the free state would result in a shortening of the time-averaged ^{15}N relaxation rate. However, the ^{15}N T_2 values are unchanged relative to those observed in isotropic solution.

At a phage concentration of 8 mg/mL and 150 mM NaCl, DinI is aligned stronger than desirable. This overalignment poses several problems: (1) measurement of residual dipolar couplings becomes less accurate because of the additional splittings that arise from ^1H-^1H dipolar couplings and concomitant lower signal to noise, (2) the transfer efficiency during INEPT segments of the NMR pulse sequences is diminished for residues where $^1D_{NH}$ and $^1D_{C\alpha H\alpha}$ approach $^1J_{NH}$ and $^1J_{C\alpha H\alpha}$, and (3) the presence of unresolved dipolar couplings to remote nuclei results in resonance broadening. These problems precluded the reliable measurement of $^1D_{C'N}$ and $^2D_{C'HN}$ couplings in the phage medium. At Pf1 concentrations below 8 mg/mL and using 150 mM NaCl, phase separation occurs over a period of several days, which disappears upon thorough mixing. So, in the presence of 150 mM NaCl, a phage concentration of 8 mg/mL is near the lower limit where a stable, aligned phase can be maintained. The electrostatic nature of DinI alignment by Pf1 phage was confirmed by titrating a 12 mg/mL Pf1 sample containing 0.6 mM DinI with NaCl. The degree of DinI alignment decreases ~30% when increasing [NaCl] from 150 to 375 mM.

The structure calculated using only the bicelle dipolar couplings is found to be in very good agreement with the dipolar couplings measured in the phage medium. Figure 7 shows a correlation between the $^1D_{C\alpha H\alpha}$ couplings measured in phage and those best fitted to the structure calculated using bicelle dipolar couplings, in addition to the NOE and torsion restraints. The high correlation coefficient ($R = 0.97$) and the absence of any areas in the protein with more pronounced differences between predicted and observed dipolar couplings confirm that DHPC binding does not significantly alter the DinI structure. Conversely, these data indicate that DinI's electrostatic interaction with the phage does not distort its structure.

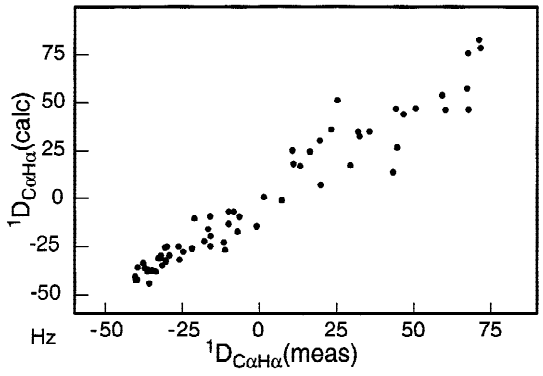

Fig. 7. Correlation between $D_{C\alpha H\alpha}$ values measured in phage medium and predicted by the structure calculated with bicelle (but no phage) dipolar coupling restraints, together with all other experimental restraints. The correlation coefficient R equals 97%.

Structure validation

The quality of the DinI NMR structure can be assessed by a quality or Q-factor based on residual dipolar couplings (Cornilescu et al., 1998; Clore & Garrett, 1999; Drohat et al., 1999). The Q-factor, a measure of the agreement between dipolar couplings predicted by the NMR structure and the measured dipolar couplings, is defined as (Cornilescu et al., 1998; Drohat et al., 1999)

$$Q = \mathrm{rms}(D_{meas} - D_{pred})/\mathrm{rms}(D_{meas}).$$

The Q-factor is somewhat analogous to the crystallographic free R-factor (Brünger, 1992). Cross-validation using residual dipolar coupling Q-factors was done as follows: A subset of residual dipolar couplings either in the same class (e.g., $^1D_{NH}$) or a mixture from the various classes is chosen randomly. This subset is generally ~10% of the total number of observed residual dipolar couplings. If for a selected coupling both phage and bicelle values are available, the subset includes both entries. Structures are calculated with all the experimental restraints, but excluding the dipolar restraints of the subset. From the resulting structures, dipolar couplings are predicted for those in the subset. The average Q-factor for the DinI NMR structure, calculated from five different randomly selected subsets of residual dipolar couplings, is 18%. This is slightly better than, for example, the agreement between the 1.8 Å X-ray crystal structure of ubiquitin (Vijay-Kumar et al., 1987) and its dipolar couplings (Ottiger & Bax, 1998b), but not as high as what can be obtained by exhaustive analysis of all NOEs, side-chain dipolar and J couplings (J.L. Marquardt, unpubl. obs.). Interestingly, the Q-factor increases several percent when the term driving backbone angles to the most populated regions of the Ramachandran map (Kuszewski et al., 1997) is excluded from the X-PLOR target function, indicating that this term actually improves the quality of the structure, and is not merely cosmetic.

Interaction with RecA

The DinI–RecA interaction inhibits the recombinase and coprotease activities of RecA, resulting in the termination of recombinational DNA repair and translesion DNA replication by the SOS response. DinI was shown to be a downregulator of the SOS response, preventing the ssDNA–RecA cofilament's promotion of the autocleavage of LexA and UmuD (Yasuda et al., 1998). Recent biochemical studies indicate that DinI can displace ssDNA from RecA (O.N. Voloshin, B.E. Ramirez, A. Bax, & R.D. Camerini-Otero, in prep.). Examination of the electrostatic potential surface of DinI indicates the presence of an extended, negatively charged ridge that is formed by residues located in the C-terminal helix of DinI, specifically: E65, E69, E72, D75, and D76 (Fig. 5B). The distribution of negative charges on this helix resembles the arrangement of negative charges in a single strand of DNA. We propose that the C-terminal helix of DinI is designed to mimic the

phosphodiester backbone of DNA, allowing DinI to compete with ssDNA for the RecA binding site. The absence of a structure of DinI complexed to RecA precludes a direct assessment of the functional significance of the kink in the C-terminal helix in the proposed binding model. However, because the spatial arrangement of the negative charges along this ridge is influenced by this kink, we expect it to be an essential feature for enhancing the complementarity between DinI and RecA. Moreover, mutagenesis data confirm the importance of E72, located in the kink, for DinI's ability to inactivate RecA in vivo (O.N. Voloshin, unpubl. obs.).

Conclusions

The structure of DinI in combination with numerous biochemical experiments (O.N. Voloshin, B.E. Ramirez, A. Bax, & R.D. Camerini-Otero, in prep.) suggests that regulation of RecA by DinI occurs through the ability of DinI to compete with ssDNA for RecA binding. The importance of the C-terminal helix of DinI in this process is highlighted by experiments that show that this helix alone is able to compete with ssDNA for binding to a peptide fragment derived from the ssDNA-binding L2 loop of RecA (O.N. Voloshin, B.E. Ramirez, A. Bax, & R.D. Camerini-Otero, in prep.). The distribution of negative charges on the surface of DinI's C-terminal kinked helix mimics the electrostatic character of a ssDNA phosphodiester backbone. We, therefore, believe that this distribution of negative charge is the primary factor that causes DinI to compete with ssDNA for the binding site on RecA. Thus, DinI appears to be yet another example of a protein that acts by mimicry of DNA. In a recent report, Liu et al. found that dTAF(II)230 can bind to TATA-box binding protein (TBP) through a surface area that mimics the widened major groove of the TATA-box found in the TBP–DNA complex (Liu et al., 1998). In another example, Selmer et al. report on a protein that mimics tRNA (Selmer et al., 1999). In both these cases, the similarity lies more in the shape than in the electrostatic properties, however. Because RecA interacts primarily with the backbone phosphate groups of DNA, the charge distribution of DinI is the primary feature that enables it to mimic DNA.

Very few homologs of DinI have been identified so far, and none have been reported in eukaryotes. However, it is conceivable that the type of charge mimicry found in DinI also occurs in other proteins that regulate activities of nonspecific nucleic acid binding proteins, both in prokaryotes and in eukaryotes.

Materials and methods

Sample preparation

The DNA encoding DinI was cloned into the pET21a vector using standard molecular biology techniques. The protein was expressed from the pET21a construct in the *E. coli* BL21(DE3) strain. Starting from a single colony taken from a freshly streaked agar plate, a 25 mL minimal medium starter culture containing ^{15}N-NH_4Cl and ^{13}C-glucose as the sole sources of nitrogen and carbon, respectively, was grown until it appeared slightly turbid ($OD_{600} \sim 1.0$), and then refrigerated overnight. The following day a 500 mL minimal medium containing ^{15}N-NH_4Cl and ^{13}C-glucose culture was inoculated with 5 mL of the starter culture. The culture was grown at 37 °C to an OD_{600} of ~0.8, at which point protein expression was induced with 1 mM IPTG. The cells were harvested after 4 h. Details regarding the purification procedure are described elsewhere (O.N. Voloshin, B.E. Ramirez, A. Bax, & R.D. Camerini-Otero, in prep.). Samples for NMR consisted of 0.6 mM DinI, 20 mM phosphate, 100 mM NaCl, 0.1% azide, and pH 6.6 (95% H_2O/5% D_2O or 99.9% D_2O), in a 250 μL Shigemi microcell.

NMR spectroscopy

All NMR experiments were performed at 25 °C, except where indicated. Data were collected on Bruker DMX500, DMX600, and DRX800 spectrometers equipped with self-shielded three-axis gradient, triple-resonance probes. All NMR data were processed with the NMRPipe package and analyzed with NMRDraw (Delaglio et al., 1995) and PIPP (Garrett et al., 1991). Sequential backbone assignments were determined from the following 3D experiments: CBCA(CO)NH, HNCACB, HNHA, ^{15}N-separated total correlation spectroscopy (TOCSY), and ^{15}N-separated NOESY (Bax & Grzesiek, 1993). Aliphatic ^{13}C and ^{1}H side-chain resonances were determined from a 3D (H)CCH-COSY experiment (Fesik et al., 1990; Kay et al., 1990; Gehring & Ekiel, 1998). Aromatic protons were assigned from 2D homonuclear COSY, TOCSY (43.5 ms mixing time), and NOESY (100 ms mixing time) experiments, recorded on a uniformly labeled ^{15}N sample in 99% D_2O at 800 MHz. In addition to $^3J_{HNH\alpha}$ measurement for obtaining ϕ constraints (Vuister & Bax, 1993), $^3J_{C'C\gamma}$ and $^3J_{NC\gamma}$ in aromatic and C^γ-methyl carrying residues were measured by quantitative J correlation spectroscopy for obtaining χ_1 angles (Grzesiek et al., 1993; Vuister et al., 1993; Hu et al., 1997). Interproton distance restraints were obtained from a 3D ^{15}N-separated NOE (100 ms mixing time) and a 3D constant-time (CT) ^{13}C-separated NOE (CT = 28 ms; mixing time = 100 ms) experiment. Interproton distance restraints involving aromatic protons were obtained from the 2D homonuclear NOESY spectrum, recorded at 800 MHz.

Residual dipolar couplings were obtained from the difference in J splittings measured in spectra of aligned and isotropic (in water at 25 °C) samples. Both bicelle and filamentous phage were used as alignment media. The bicelle medium contained 50 mg/mL lipids in the molar ratio of DTPC:DHPC:CTAB = 30:10:1 (DTPC ditridecanoylphosphocholine; DHPC, dihexanoylphosphocholine; CTAB, cetyltrimethylammonium bromide). All NMR experiments on the bicelle sample were recorded at 28 °C because 25 °C was found to be too close to the temperature where the liquid crystal is no longer stable. The phage LC sample contained 8 mg/mL Pf1 phage. All NMR experiments on the phage LC sample were also recorded at 28 °C to slightly reduce the degree of alignment and improve protein linewidth. $^1D_{NH}$ residual dipolar couplings were obtained from ^{1}H-coupled (F1) IPAP {^{15}N,^{1}H}-HSQC experiments (Ottiger et al., 1998). $^1D_{NC'}$ and $^2D_{C'HN}$ residual dipolar couplings were obtained from ^{1}H,^{13}C′-coupled (F1) IPAP {^{15}N,^{1}H}-HSQC experiments (Wang et al., 1998). $^1D_{C\alpha H\alpha}$ residual dipolar couplings were obtained from 3D CT-(H)CA(CO)NH experiments without ^{1}H-decoupling in the F_1 dimension (Tjandra & Bax, 1997b). $^1D_{C\alpha C'}$ residual dipolar couplings were obtained from 3D $^{13}C^\alpha$-coupled HNCO experiments. Because the ^{13}C′ linewidth is dominated by chemical shift anisotropy, these HNCO spectra were recorded at the lowest field strength (500 MHz ^{1}H frequency), yielding narrower linewidths but, nevertheless, adequate resolution.

Structure calculations

Distance calibration of the interproton distance constraints obtained from the 3D ^{15}N-separated NOESY experiment was done as follows: All non-Gly residues in the allowed negative ϕ region

have H^N_{i-1}-H^α_i distances of 2.9 ± 0.2 Å. Other interproton distances were scaled relative to this average 2.9 Å distance using an empirical $1/r^4$ dependence of the intensity, which in a very approximate manner accounts for the effects of spin diffusion (Güntert et al., 1991). Distance ranges were set to ±25% of the target distance, except for degenerate peaks. For degenerate peaks, no lower distance bound was used, and $1/r^6$ averaging was employed in simulated annealing calculations (Clore et al., 1986). Distance calibration of the interproton distance restraints obtained from the 3D ^{13}C-separated NOESY-CT-HSQC experiment was done as follows: For NOEs to methyl groups (detected during t_3), the average NOE intensity from the adjacent vicinal methine proton to the methyl group in Ile, Thr, Ala, and Val residues was used as a reference [$(\sum_i r_i^{-6})^{-1/6}$ = 2.1 Å]. For nonmethyl ^{1}H signals, the average intraresidue H^NH^α cross peak to diagonal peak intensity ratio is used as a 2.9 Å reference distance, again using an empirical $1/r^4$ distance dependence, and relatively tight ±25% tolerances. No lower bound distance was given for degenerate peaks and residues with extensive conformational averaging (as evidenced by very intense ^{1}H-^{13}C correlations in the CT-HSQC spectrum). Interproton distance restraints derived from the 2D homonuclear NOESY experiment were grouped into five overlapping classes 2.0–2.7, 2.3–3.2, 2.7–3.7, 3.0–4.5, and 3.3–5.5 Å, corresponding to very strong, strong, medium, weak, and very weak NOEs, respectively. Degenerate peaks were also classified using these intensity classifications, except no lower distance bound was employed.

Structures were calculated by simulated annealing using the program X-PLOR (Brünger, 1993) adapted to incorporate residual dipolar coupling restraints (Tjandra et al., 1997) and a conformational database (Kuszewski et al., 1997). The minimized target function comprises harmonic potentials for covalent geometry (bonds, angles, and improper torsions) and residual dipolar coupling restraints, quadratic square-well potentials for interproton distance and dihedral angle restraints, and a quartic van der Waals repulsion term for nonbonded contacts. Force constants are listed in the footnote to Table 1. Initial folds were calculated in Cartesian coordinate space starting from a completely extended structure using only NOE restraints and backbone dihedral angle restraints derived from the program TALOS (Cornilescu et al., 1999). TALOS restraints were available for 60 residues. All 20 residues for which no unambiguous TALOS restraints were obtained fall outside regions of regular secondary structure. Also, χ_1 angle restraints were derived for most Val, Ile, Thr, and aromatic residues from $^3J_{C'C\gamma}$ and $^3J_{NC\gamma}$ values. The 10 lowest energy structures were used as input for a second simulated annealing calculation that included residual dipolar coupling restraints measured in the bicelle medium, together with all NOE restraints. TALOS backbone dihedral angle restraints were not used in this second stage. Instead, 42 ϕ dihedral angle restraints were derived from $^3J_{HNH\alpha}$ values, aided by the finding that for all non-Gly residues $^1J_{C\alpha H\alpha} \geq$ 139 Hz, indicating $\phi < 0$ (Vuister et al., 1992). For non-Gly residues without an unambiguous $^3J_{HNH\alpha}$-derived ϕ restraint but with $^1J_{C\alpha H\alpha} \geq$ 139 Hz, only the less restrictive $\phi < 0$ restraint was used. In fact, the smallest $^1J_{C\alpha H\alpha}$ measured was 140 Hz for T6. These $^1J_{C\alpha H\alpha}$ values are a byproduct of the $^1D_{C\alpha H\alpha}$ measurement, but nevertheless greatly improve convergence during the early stages of the structure calculation. A total of 51 loose ψ restraints were derived from the corresponding intraresidue and sequential H^α-H^N NOE intensity ratios. The 10 lowest energy structures from the initial round of calculations were used as starting structures in a final refinement stage that included both the bicelle and phage dipolar restraints, together with NOE and experimental dihedral angle restraints.

Data have been deposited in the PDB (accession number 1F0A)

Acknowledgments

We thank Marius Clore, Georg Kontaxis, and John Marquardt for useful discussions and Frank Delaglio, Dan Garrett, and Markus Zweckstetter for software support. B.E.R. is supported by a postdoctoral fellowship from the National Science Foundation (DBI-9807412).

References

Bax A, Grzesiek S. 1993. Methodological advances in protein NMR. *Acc Chem Res 26*:131–138.

Brünger AT. 1992. Free R-value—A novel statistical quantity for assessing the accuracy of crystal-structures. *Nature 355*:472–475.

Brünger AT. 1993. *X-PLOR manual version 3.1*. New Haven, Connecticut: Yale University.

Clore GM, Brünger AT, Karplus M, Gronenborn AM. 1986. Application of molecular-dynamics with interproton distance restraints to 3-dimensional protein-structure determination—A model study of crambin. *J Mol Biol 191*:523–551.

Clore GM, Garrett DS. 1999. R-factor, free R, and complete cross-validation for dipolar coupling refinement of NMR structures. *J Am Chem Soc 121*:9008–9012.

Clore GM, Gronenborn AM, Bax A. 1998a. A robust method for determining the magnitude of the fully asymmetric alignment tensor of oriented macromolecules in the absence of structural information. *J Magn Reson 133*:216–221.

Clore GM, Starich MR, Bewley CA, Cai ML, Kuszewski J. 1999. Impact of residual dipolar couplings on the accuracy of NMR structures determined from a minimal number of NOE restraints. *J Am Chem Soc 121*:6513–6514.

Clore GM, Starich MR, Gronenborn AM. 1998b. Measurement of residual dipolar couplings of macromolecules aligned in the nematic phase of a colloidal suspension of rod-shaped viruses. *J Am Chem Soc 120*:10571–10572.

Cornilescu G, Delaglio F, Bax A. 1999. Protein backbone angle restraints from searching a database for chemical shift and sequence homology. *J Biomol NMR 13*:289–302.

Cornilescu G, Marquardt JL, Ottiger M, Bax A. 1998. Validation of protein structure from anisotropic carbonyl chemical shifts in a dilute liquid crystalline phase. *J Am Chem Soc 120*:6836–6837.

Cox MM. 2000. Recombinational DNA repair in bacteria and the RecA protein. *Prog Nucleic Acid Res Mol Biol 63*:311–366.

Delaglio F, Grzesiek S, Vuister GW, Zhu G, Pfeifer J, Bax A. 1995. Nmrpipe—A multidimensional spectral processing system based on unix pipes. *J Biomol NMR 6*:277–293.

Drohat AC, Tjandra N, Baldisseri DM, Weber DJ. 1999. The use of dipolar couplings for determining the solution structure of rat apo-S100B (beta beta). *Protein Sci 8*:800–809.

Fesik SW, Eaton HL, Olejniczak ET, Zuiderweg ERP, McIntosh LP, Dahlquist FW. 1990. 2D and 3D NMR-spectroscopy employing C-13-C-13 magnetization transfer by isotropic mixing—Spin system-identification in large proteins. *J Am Chem Soc 112*:886–888.

Friedberg EC, Walker GC, Siede W. 1995. *DNA repair and mutagenesis*. Washington, DC: ASM Press.

Garrett DS, Powers R, Gronenborn AM, Clore GM. 1991. A common-sense approach to peak picking in 2-dimensional, 3-dimensional, and 4-dimensional pectra using automatic computer-analysis of contour diagrams. *J Magn Reson 95*:214–220.

Gehring K, Ekiel I. 1998. H(C)CH-COSY and (H)CCH-COSY experiments for C-13-labeled proteins in H_2O solution. *J Magn Reson 135*:185–193.

Grzesiek S, Bax A, Hu JS, Kaufman J, Palmer I, Stahl SJ, Tjandra N, Wingfield PT. 1997. Refined solution structure and backbone dynamics of HIV-1 Nef. *Protein Sci 6*:1248–1263.

Grzesiek S, Vuister GW, Bax A. 1993. A simple and sensitive experiment for measurement of Jcc couplings between backbone carbonyl and methyl carbons in isotopically enriched proteins. *J Biomol NMR 3*:487–493.

Güntert P, Braun W, Wüthrich K. 1991. Efficient computation of 3-dimensional protein structures in solution from nuclear-magnetic-resonance data using the program Diana and the supporting programs Caliba, Habas and Glomsa. *J Mol Biol 217*:517–530.

Hansen MR, Mueller L, Pardi A. 1998. Tunable alignment of macromolecules by filamentous phage yields dipolar coupling interactions. *Nat Struct Biol 5*:1065–1074.

Holm L, Sander C. 1993. Protein–structure comparison by alignment of distance matrices. *J Mol Biol 233*:123–138.

Hu JS, Grzesiek S, Bax A. 1997. Two-dimensional NMR methods for determining (chi 1) angles of aromatic residues in proteins from three-bond J(C′C gamma) and J(NC gamma) couplings. *J Am Chem Soc 119*:1803–1804.

Kay LE, Ikura M, Bax A. 1990. Proton proton correlation via carbon carbon couplings—A 3-dimensional NMR approach for the assignment of aliphatic resonances in proteins labeled with C-13. *J Am Chem Soc 112*:888–889.

Koradi R, Billeter M, Wüthrich K. 1996. MOLMOL: A program for display and analysis of macromolecular structures. *J Mol Graphics 14*:51.

Kuszewski J, Gronenborn AM, Clore GM. 1997. Improvements and extensions in the conformational database potential for the refinement of NMR and X-ray structures of proteins and nucleic acids. *J Magn Reson 125*:171–177.

Laskowski RA, Macarthur MW, Moss DS, Thornton JM. 1993. Procheck—A program to check the stereochemical quality of protein structures. *J Appl Crystallogr 26*:283–291.

Liu DJ, Ishima R, Tong KI, Bagby S, Kokubo T, Muhandiram DR, Kay LE, Nakatani Y, Ikura M. 1998. Solution structure of a TBP-TAF(II)230 complex: Protein mimicry of the minor groove surface of the TATA box unwound by TBP. *Cell 94*:573–583.

Nicholls A, Sharp KA, Honig B. 1991. Protein folding and association—Insights from the interfacial and thermodynamic properties of hydrocarbons. *Proteins Struct Funct Genet 11*:281–296.

Ottiger M, Bax A. 1998a. Characterization of magnetically oriented phospholipid micelles for measurement of dipolar couplings in macromolecules. *J Biomol NMR 12*:361–372.

Ottiger M, Bax A. 1998b. Determination of relative N-H-N N-C′, C-alpha-C′, and C(alpha)-H-alpha effective bond lengths in a protein by NMR in a dilute liquid crystalline phase. *J Am Chem Soc 120*:12334–12341.

Ottiger M, Delaglio F, Bax A. 1998. Measurement of J and dipolar couplings from simplified two-dimensional NMR spectra. *J Magn Reson 131*:373–378.

Ottiger M, Tjandra N, Bax A. 1997. Magnetic field dependent amide N-15 chemical shifts in a protein–DNA complex resulting from magnetic ordering in solution. *J Am Chem Soc 119*:9825–9830.

Ramirez BE, Bax A. 1998. Modulation of the alignment tensor of macromolecules dissolved in a dilute liquid crystalline medium. *J Am Chem Soc 120*:9106–9107.

Sanders CR, Schwonek JP. 1992. Characterization of magnetically orientable bilayers in mixtures of dihexanoylphosphatidylcholine and dimyristoylphosphatidylcholine by solid-state NMR. *Biochemistry 31*:8898–8905.

Selmer M, Al-Karadaghi S, Hirokawa G, Kaji A, Liljas A. 1999. Crystal structure of *Thermotoga maritima* ribosome recycling factor: A tRNA mimic. *Science 286*:2349–2352.

Shinagawa H, Iwasaki H, Kato T, Nakata A. 1988. RecA protein-dependent cleavage of UmuD protein and Sos mutagenesis. *Proc Natl Acad Sci USA 85*:1806–1810.

Struppe J, Vold RR. 1998. Dilute bicellar solutions for structural NMR work. *J Magn Reson 135*:541–546.

Subramanya HS, Roper DI, Dauter Z, Dodson EJ, Davies GJ, Wilson KS, Wigley DB. 1996. Enzymatic ketonization of 2-hydroxymuconate: Specificity and mechanism investigated by the crystal structures of two isomerases. *Biochemistry 35*:792–802.

Sugimoto H, Taniguchi M, Nakagawa A, Tanaka I, Suzuki M, Nishihira J. 1999. Crystal structure of human D-dopachrome tautomerase, a homologue of macrophage migration inhibitory factor, at 1.54 angstrom resolution. *Biochemistry 38*:3268–3279.

Tjandra N, Bax A. 1997a. Direct measurement of distances and angles in biomolecules by NMR in a dilute liquid crystalline medium. *Science 278*:1111–1114.

Tjandra N, Bax A. 1997b. Large variations in C-13(alpha) chemical shift anisotropy in proteins correlate with secondary structure. *J Am Chem Soc 119*:9576–9577.

Tjandra N, Omichinski JG, Gronenborn AM, Clore GM, Bax A. 1997. Use of dipolar H-1–N-15 and H-1–C-13 couplings in the structure determination of magnetically oriented macromolecules in solution. *Nat Struct Biol 4*:732–738.

Vijay-Kumar S, Bugg CE, Cook WJ. 1987. Structure of ubiquitin refined at 1.8 A resolution. *J Mol Biol 194*:531–544.

Vold RR, Prosser RS, Deese AJ. 1997. Isotropic solutions of phospholipid bicelles: A new membrane mimetic for high-resolution NMR studies of polypeptides. *J Biomol NMR 9*:329–335.

Vuister GW, Bax A. 1993. Quantitative J correlation—A new approach for measuring homonuclear 3-bond J(H(N)H(Alpha) coupling-constants in N-15-enriched proteins. *J Am Chem Soc 115*:7772–7777.

Vuister GW, Delaglio F, Bax A. 1992. An empirical correlation between 1J(Ca-Ha) and protein backbone conformation. *J Am Chem Soc 114*:9674–9675.

Vuister GW, Wang AC, Bax A. 1993. Measurement of 3-bond nitrogen carbon-J couplings in proteins uniformly enriched in N-15 and C-13. *J Am Chem Soc 115*:5334–5335.

Walker GC. 1998. Skiing the black diamond slope: Progress on the biochemistry of translesion DNA synthesis. *Proc Natl Acad Sci USA 95*:10348–10350.

Wang YX, Marquardt JL, Wingfield P, Stahl SJ, Lee-Huang S, Torchia D, Bax A. 1998. Simultaneous measurement of H-1–N-15, H-1–C-13′, and N-15–C-13′ dipolar couplings in a perdeuterated 30 kDa protein dissolved in a dilute liquid crystalline phase. *J Am Chem Soc 120*:7385–7386.

Yasuda T, Morimatsu K, Horii T, Nagata T, Ohmori H. 1998. Inhibition of *Escherichia coli* RecA coprotease activities by DinI. *EMBO J 17*:3207–3216.

Zweckstetter M, Bax A. 2000. Prediction of sterically induced alignment in a dilute liquid crystalline phase: Aid to structure determination by NMR. *J Am Chem Soc 122*:3791–3792.